Sandwich domain walls in cordierite: a computer simulation study

1999 J. Phys.: Condens. Matter 11 4747

(http://iopscience.iop.org/0953-8984/11/24/315)

J. Phys.: Condens. Matter **11** (1999) 4747–4766. Printed in the UK PII: S0953-8984(99)96580-3

Sandwich domain walls in cordierite: a computer simulation study

John F Blackburn and Ekhard K H Salje

Department of Earth Sciences, University of Cambridge, Downing Street, Cambridge CB2 3EQ, UK

Received 6 August 1998, in final form 18 March 1999

Abstract. Below T_c, cordierite shows an unusual domain pattern consisting of walls which are not well oriented along elastic soft directions. This is due to a low spontaneous strain and low anisotropy energies. As a result of this, short-ranging interactions normally negligible compared to strain energies become important and there is a competition between two types of wall: those due to strain and those due to local interactions. This leads to the formations of 'sandwich walls', which represent a compromise between these two wall types, becoming energetically favourable. Here we simulate the formation of sandwich walls using an atomistic computer model. The sandwich walls are shown to be chiral in nature with a vector order parameter rotating as we move through the wall. The chirality direction is fixed since the two chirality types are not degenerate. The sandwich wall trajectories are similar to what would be expected from symmetry-adapted Ginzburg–Landau theory. The sandwich 'filling' appears in two shapes: a thick, well defined domain at low temperatures and a thin layer of wetting at higher temperatures. The latter is reminiscent of surface segregation phenomena.

1. Introduction

Below a critical temperature, T_c, most ferroelastic materials show the formation of domain patterns. The walls between adjacent domains tend to be aligned along elastic soft directions such that the elastic strain tensors in the adjacent domains are compatible without the formation of secondary strain fields [1–3]. In most ferroelastics, this tendency is very strong with almost all walls located along such soft directions. These walls tend to be very straight and clearly defined with little deviation from the soft direction.

Cordierite, on the other hand shows a very complex, patchy microstructure with poorly defined wiggly domain walls and blunt needle domains [4, 5]. Although there is a tendency for walls to align along soft directions, this appears to be much weaker than in other ferroelastics and some walls are observed which are not along elastically soft directions. These walls do, however, seem to be along *particular* directions. In a previous paper [6] we suggested a mechanism by which this type of ordering could occur based on short-ranging interactions between cordierite's characteristic sixfold tetrahedral ring structure. This mechanism involves local, *topological* interactions which are usually masked out in ferroelastics due to the strong, long-ranging elastic interactions which are themselves independent of detailed atomic structure. They assume a greater importance in cordierite due to its weak elastic interactions and small spontaneous strain.

There are, then, two types of competing wall formation in cordierite, strain-mediated elastic walls and topological walls which result from local interactions. One can therefore

0953-8984/99/244747+20$19.50

imagine a low-energy wall configuration which would satisfy cordierite's tendency to form topological walls on a short scale but strain walls on a higher length scale. We call such a wall a *sandwich wall*. Viewed from a distance, it appears to be a simple strain wall but closer inspection reveals additional 'decoration' inside the wall such that the actual interfaces that form inside the 'wall' are two topological walls. We will describe the detail of this structure in the next section. Since such sandwich walls have a low energy it is possible that many walls in cordierite which appear to be strain walls when viewed under an optical microscope are in fact these sandwich walls.

In this paper we use a computer simulation to model domain formation in cordierite and show how both strain and topological walls can form. We then consider the particular case of a sandwich wall in detail at different temperatures. These computational results are then compared with the theoretical results of Ginzburg–Landau theory giving us a better understanding of the mechanisms involved. In the GL theory we can describe the wall shape using a vector order parameter, $\boldsymbol{Q}$, which rotates in Q-space as we move through the wall. The precise direction of rotation dictates the *chirality* of the wall and the nature of such chiral walls has been studied in the past often on a purely abstract level [7]. In this paper we reconcile the sandwich wall shapes (whose chirality has a direct physical meaning) with such analyses.

2. Cordierite structure

The structure of cordierite is illustrated in figure 1 [8]. It consists of two types of oxygen tetrahedron called T1 and T2. The T2 tetrahedra form layers of six-membered rings. In each unit cell there are two layers of T2 rings with the rings in alternate layers rotated by 30° with respect to each other. The T1 tetrahedra form 'ladders' connecting these T2 layers. There are also oxygen octahedra present between the T1 tetrahedra with Mg atoms at their centres. Al or Si atoms are present in each tetrahedron and the precise configuration of Al/Si dictates the ordering of the crystal. Hence these atoms are called *ordering atoms* and the remainder of the lattice (comprising O and Mg atoms) is called the *host lattice*.

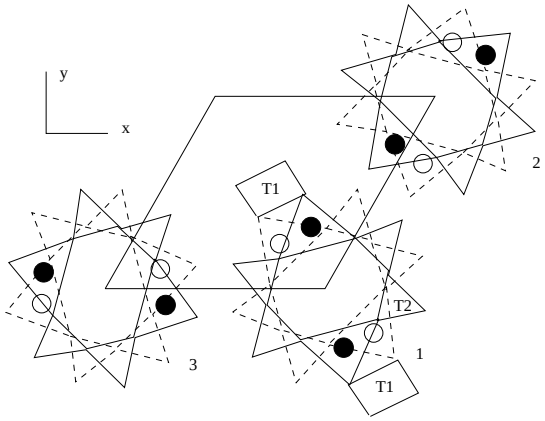

Figure 1. The numbering system used to indicate Al opposite pair configurations in each ring. The axes shown are used throughout. The two types of T2 ring per unit cell are shown as solid and dashed lines. They are each made up of T2 tetrahedra shown here as triangles. The Al positions are shown as black and white circles respectively. Other tetrahedra have Si atoms at their centres.

Al atoms are physically larger than Si atoms and so, when Al are present, they cause their tetrahedra to swell up distorting the host lattice. These distortions propagate throughout the

crystal and apply forces on other ordering atoms. So ordering atoms interact with each other indirectly via the host lattice.

Domain formation occurs when each T2 ring contains two Al and four Si atoms and the Al atoms are aligned on opposite sides of the ring. There are three ways of having this type of order and so there are three types of domain. Each ring has a domain type associated with it which we will denote by a number 1, 2 or 3. We will call this number the *ring spin* since it is analogous with spins found in ferromagnetic materials. In using this nomenclature we reduce the system to a three-state Potts model in three dimensions [9, 10].

There is a tendency to exclude two Al from being present in adjacent tetrahedra (Loewenstein's rule [11]), so the 'spin' of a ring indicates the configuration of ordering atoms in that T2 ring and also in the *surrounding* ring of T1 tetrahedra. Thus the configuration of all ordering atoms in the crystal can be specified by stating the ring spin configuration. The three types of ring ordering are illustrated in figure 1. Notice how the Al opposite pairs in the two types of T2 ring are aligned next to each other such that the Al-bearing T2 sites on each side of the ring are connected by T1 tetrahedra. The diagram also shows how T2 tetrahedra with Al present swell up, distorting the T2 ring into an elliptical shape with one axis along the Al opposite pair direction.

Cordierite undergoes a phase transition from hexagonal ($P6/mcc$) to orthorhombic ($Cccm$) structure. The spontaneous strain has the symmetry of the active representation (E_{2g}) and is given by

$$\mathbf{e} = e\begin{pmatrix} 1 & 0 & 0 \\ 0 & -1 & 0 \\ 0 & 0 & 0 \end{pmatrix} \tag{1}$$

with respect to the strain's principal axes in each of the three domain types. This strain is just what one would expect from the ring distortion shown in figure 1.

When two domains come together, the interface is called a *domain wall*. If the wall is strain mediated, its orientation must be such that the strain a small distance away from the wall is the same in both adjacent domains [1–3]. Using this condition for a hexagonal/orthorhombic system, six walls of fixed direction perpendicular to the T2 planes are obtained; these are listed in table 1.

Table 1. Six walls of fixed direction perpendicular to the T2 planes.

Domain pair	Wall 1 angle	Wall 2 angle
1–2	0	+ 90°
1–3	+ 60°	−30°
2–3	−60°	+ 30°

These walls are shown schematically in the lower part of figure 2. As required by strain interactions, there are two mutually orthogonal walls for each domain pair. Structurally, the strain wall directions are located halfway between the Al opposite pair orientations. The diagram also shows the topological wall directions. The topological walls are located along the Al opposite pair directions.

A sandwich wall consists of two domains which would form a strain wall if directly connected but with a slice of the other domain type in between, so the actual domain interfaces are topological in nature. Figure 3 illustrates such a wall.

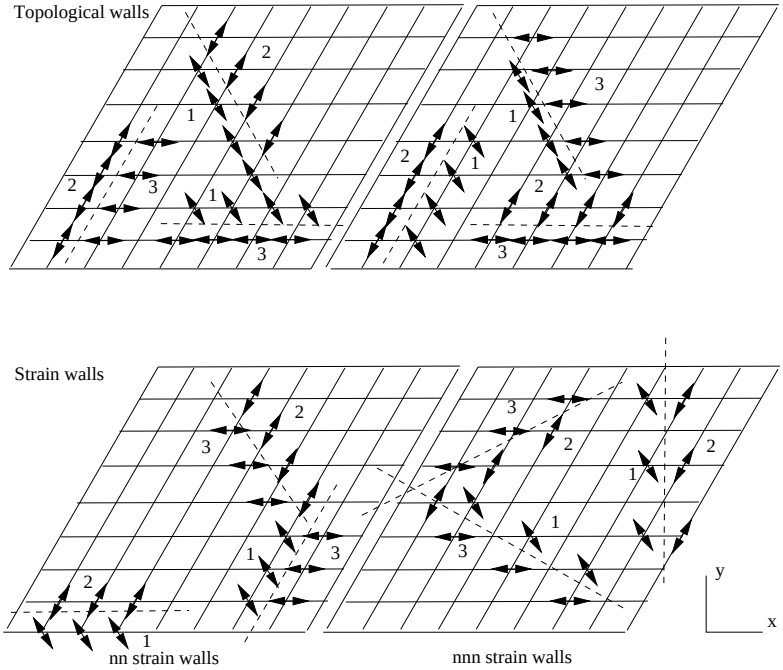

Figure 2. The six strain walls and six topological walls observed in the simulation. A T2 ring is present at each line intersection in the diagram. The double-headed arrows indicate the direction of alignment of the opposite pairs of Al in the rings. In fact the actual Al positions are rotated by $\pm 15^{\circ}$ with respect to the arrow direction for the two non-equivalent T2 layers shown in figure 1. The arrow is drawn halfway between these two orientations and also corresponds to the strain direction. The dashed lines indicate the wall directions.

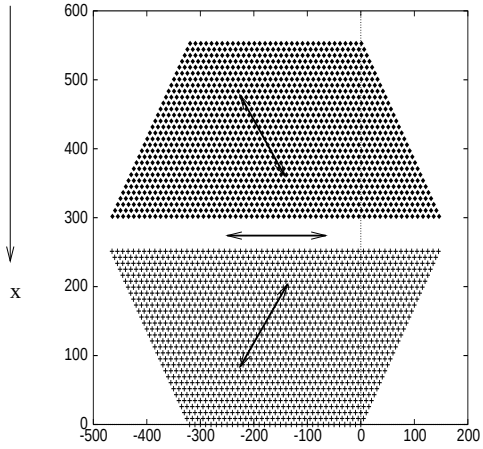

Figure 3. A sandwich wall. The circles are type 1 ring spins, crosses are type 2 and type 3 are not shown (white).

3. Computer model

In the computer model, we simulate a structure which is the direct analogue of cordierite but in 2D. As strain interactions are rather well reproduced in 2D, it is only the local interactions

which may be oversimplified in this representation.

Looking at the 3D structure defined in figure 1, we imagine rotating the two types of T2 ring together and, at the same time, compressing them into a 2D sheet as shown in figure 4. The T2 tetrahedra become triangles and the T1s become single lines connecting the T2 tetrahedra in neighbouring rings.

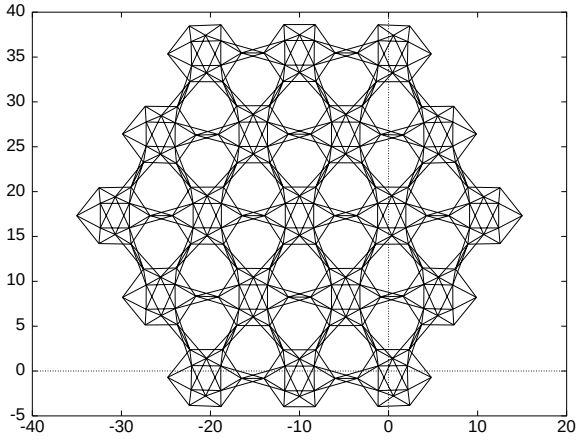

Figure 4. The 2D structural model. The lines represent springs connecting oxygen atoms. This sample consists of a single type 3 domain and we can see that the T2 triangles containing Al are swollen with a consequent distortion of the rings causing the crystal to lose symmetry and become orthorhombic. The model used in the simulations has 32 rings on a side of the hexagonal sample rather than the 3 shown here.

As stated in the previous section, we can identify two distinct sublattices in cordierite, the host lattice (consisting of O and Mg atoms) and the ordering lattice (consisting of Al and Si atoms). In the computer model, the host atoms interact via harmonic forces (i.e. they are connected by springs). The ordering atoms interact with the host atoms by applying constant *Kanzaki* forces on the host atoms depending on which type of ordering atom is present. Since Al atoms are larger than Si atoms, we model this interaction by saying that Al atoms apply outward forces on oxygen atoms in their tetrahedra while Si atoms apply no forces. The direct interaction between ordering atoms is assumed to negligible in this simulation and is set at zero.

The connectivity and strength of springs must be chosen to give the right interactions between host atoms. These springs are shown as lines in figure 4. The tetrahedra in these ferroelastic materials are known to be rather rigid and so the oxygen atoms at the vertices of the T2 triangles are connected together using relatively strong springs ($k = 100$ relative units). When Kanzaki forces are applied to the oxygens at the edges of these tetrahedra, they swell up until the restoring force due to these springs equals the Kanzaki force.

The line which is all that remains of the T2 rings is also expressed as a spring ($k = 100$ relative units). In this form, the T2 ring would be very floppy and we expect it to behave as a fairly well defined rigid unit, so additional springs ($k = 50$ relative units) are added inside and outside the ring to stabilize its structure. Finally, some additional springs are connected between rings to increase the ring–ring interaction ($k = 200$ relative units). The resulting system is shown in figure 4.

This simulation incorporates all of the physical mechanisms believed to be important in cordierite ordering: the swelling of 'tetrahedra' (now triangles) in the presence of Al, the consequent distortion of the T2 rings into ellipses and the interaction between distorted rings

which causes strain and hence ordering.

The Hamiltonian of this system can be written as

$$H = H_{host} + H_{int} \tag{2}$$

where H_{host} is the energy of the host-atom–host-atom interactions and H_{int} is the energy of the ordering-atom–host-atom interactions due to the Kanzaki forces applied [12]. We assume that ordering-atom–ordering-atom interactions are irrelevant to the total energy.

Because we are using simple spring bonds for the host lattice, we can write H_{host} as

$$H_{host} = \sum_{bonds} \frac{1}{2} k_{bond} (\delta r)^2 \tag{3}$$

where δr is the stretching of a bond and k_{bond} is the spring constant. The sum is over all bonds in the host lattice. Using the formalism of the dynamical matrix we can rewrite this as

$$H_{host} = \frac{1}{2} \boldsymbol{u}^{\mathrm{T}} \mathbf{A} \boldsymbol{u} = \frac{1}{2} \sum_{nm} \sum_{ij} u_n^i A_{nm}^{ij} u_m^j \tag{4}$$

with the first expression written in matrix format (the matrices must be appropriately partitioned so as to include the indices n, m, i, j). u_n^i is the ith displacement component of atom n and A_{nm}^{ij} represents the spring interaction between the ith and jth displacement components of atoms n and m.

The force on each host atom, n, denoted f_n^i (with i corresponding to the Cartesian component) is given by

$$f_n^i = \sum_{l\alpha} F_{nl}^{i\alpha} p_l^{\alpha} \tag{5}$$

where p_l^{α}, the so-called occupation number, indicates the presence or absence of an ordering atom of type α at site l such that $p = 1$ if the atom is present and $p = 0$ if the spin is absent. In cordierite, we take $p_l^1 = 1$ for an Al and $p_l^0 = 1$ for a Si at site l. The matrix element $F_{nl}^{i\alpha}$ represents the ith component of the force applied to host atom n when an ordering atom of type α is present at site l. The matrix $\mathbf{F}$ therefore gives the set of Kanzaki forces.

Since the Kanzaki forces are constant, we can now write the total Hamiltonian as

$$H = \frac{1}{2} \boldsymbol{u}^{\mathrm{T}} \mathbf{A} \boldsymbol{u} - \boldsymbol{u}^{\mathrm{T}} \mathbf{F} \boldsymbol{p} = \frac{1}{2} \sum_{nm} \sum_{ij} u_n^i A_{nm}^{ij} u_m^j - \sum_{nl} \sum_{i} \sum_{\alpha} u_n^i F_{nl}^{i\alpha} p_l^{\alpha}. \tag{6}$$

The evolution of the ordering-atom configuration is modelled using the standard Metropolis algorithm of Monte Carlo analysis, changes of ring spins (which correspond to *rotating* pairs of Als) are attempted and the attempts accepted with probability

$$p(\Delta E) = \frac{\exp(-\Delta E / k_B T)}{1 + \exp(-\Delta E / k_B T)}. \tag{7}$$

Thus the system performs a 'random walk' from its initial configuration. Making use of the ergodic nature of the system, we can take the evolution of the system as it 'walks' to correspond to its *time evolution*. The number of Monte Carlo steps, t_{MC}, is related to the real time elapsed, t, by

$$t = t_{MC} \exp(E_a / k_B T) \tag{8}$$

where E_a is some characteristic activation energy of the Monte Carlo interchange. Thus a sequence of spin-configuration snapshots represents the time evolution of the system.

In the computer simulation we are only interested in the motion of the ordering atoms since these dictate domain formation. The host atoms are necessary only as an elastic medium

with the required stiffness and geometry to cause the correct interactions between ordering atoms. In order to express this interaction most clearly, we allow the host lattice to relax to its minimum-energy configuration between changes of ring spins. This also allows us to eliminate the host-atom displacements from equation (6) and hence reduce the model to a Potts model.

Minimizing (6) with respect to atomic displacements gives

$$\frac{\partial H}{\partial u_n^i} = (\mathbf{A}\boldsymbol{u} - \mathbf{F}\boldsymbol{p})_n^i = 0 \tag{9}$$

which leads to the matrix of relaxed displacements:

$$(u_0)_n^i = (\mathbf{A}^{-1}\mathbf{F}\boldsymbol{p})_n^i. \tag{10}$$

Substituting this back into (6) yields

$$H_0 = \frac{1}{2}\boldsymbol{p}^{\mathrm{T}}\mathbf{V}\boldsymbol{p} \tag{11}$$

with

$$V_{lk}^{\alpha\beta} = -(\mathbf{F}^{\mathrm{T}}\mathbf{A}^{-1}\mathbf{F})_{lk}^{\alpha\beta}. \tag{12}$$

This is the Hamiltonian used in the simulation. It is formally the same as that of a Potts model with a complex interaction term $\mathbf{V}$. While in nearest-neighbour Potts models most elements of $\mathbf{V}$ are zero, *none* of the elements are zero in our simulation. In fact, the interaction can be shown to decrease as R^3 where R is the distance between ordering atoms, so it is indeed long ranging as we expect. The anisotropy of the interaction of the system can also be derived from an analysis of equation (11) [13].

One way to calculate the energy differences required for the Metropolis algorithm would be to calculate the tensor V from the springs and Kanzaki forces of the system. However, the number of atoms considered in these simulations is large (of order 10^4) and the size of the dynamical matrix $\mathbf{A}$ is $(dN)^2$ where d is the dimensionality and N the number of host atoms. It is impractical to invert such a large matrix and so Newtonian molecular dynamics with damping is used to move the host atoms to their lowest energy positions and minimize the energy in equation (6).

The most straightforward way to proceed would be to calculate the energy for a relaxed system (using molecular dynamics), interchange ordering atoms, recalculate the energy and subtract to get the energy change for equation (7). However, the relaxation process for such a large number of atoms is very computationally intensive and doing two relaxations per interchange requires too long a computational time.

Instead of calculating ΔE directly, we calculate the quantity

$$\Delta\tilde{E} = -\boldsymbol{u}_0\mathbf{F}\,\Delta\boldsymbol{p} \tag{13}$$

where u_0 is the set of relaxed host-atom displacements corresponding to an initial ring spin configuration and Δp is the difference in the ring spin due to one Monte Carlo interchange. This quantity turns out to be related to ΔE by

$$\Delta E = \Delta\tilde{E} + \delta \tag{14}$$

where δ is the so-called *energy correction*. It is a constant which depends only the structure of the model.

From a comparison of equations (11) and (13), it can be shown that δ can be calculated from the following configurations. If we consider a particular ring at the centre of a hexagonal sample and imagine that the rest of the lattice apart from this ring contains no ordering atoms (and so no Kanzaki forces are applied to the atoms in other rings), then E_0 is the relaxed energy of a single Al placed at any of the six sites in this ring (all six sites are symmetrically identical).

E_1 is the energy of two Als placed next to each other in the ring; E_2 is the energy of two Als placed next *but one* to each other and E_{opp} is the energy of two Als placed opposite each other (just like in an ordered system). The energy correction can then be shown to be given by

$$\delta = 8E_0 + 2E_{opp} - 2E_1 - 2E_2 \tag{15}$$

and this quantity was calculated at the outset and used in each simulation presented here.

The computer algorithm then operates as follows: the host lattice is relaxed, *all* Monte Carlo changes in the lattice are attempted at once and the process is repeated. Thus all of the ring spins can be changed for a single host-lattice relaxation.

We use free boundary conditions throughout rather than the more usual periodic boundaries because the latter tend produce a spurious periodicity in the spin configurations generated by the simulation. Periodic boundaries also prevent the formation of large-wavelength stretching modes in the host lattice, which we expect to be important due to the long-ranging nature of the elastic interaction.

The computer programs were run on the Hitachi S-3600 vector computer, part of the Cambridge University High Performance Computing Facility.

4. Computer results from a random configuration

To establish at which temperatures to run the simulation, we must first calculate T_c. This is done by defining a vector, $\boldsymbol{q}$, for each ring spin:

$$\boldsymbol{q}_i = (\cos[(2\pi/3)(s_i - 1)], \sin[(2\pi/3)(s_i - 1)]) \tag{16}$$

where s_i is the ring spin value as defined in figure 1. The order parameter is now given as the ensemble-averaged normalized magnetization:

$$Q = \langle Q_m \rangle \tag{17}$$

$$Q_m = \frac{1}{N}\left|\sum_i \boldsymbol{q}_i\right|. \tag{18}$$

In practice the system is ergodic, so we calculate the Monte Carlo average of Q_m rather than an ensemble average. Figure 5 shows a plot of $Q(T)$ for several temperatures; in each case the magnetization is averaged over 1000 Monte Carlo steps per ring spin which gives a good convergence. We see that the order parameter remains very close to 1 up to quite close to the critical temperature, T_c, and then rapidly decreases to zero. This sharp cut-off is reminiscent of $(T - T_c)^{1/8}$ curves resulting from nearest-neighbour Ising models, showing that short-ranging interactions (which will yield the topological walls) have a strong effect on ordering. Also shown on the graph is corresponding plot of the order parameter for a simple model with one atom per unit cell which was also simulated. This latter plot is close to the $(T - T_c)^{1/2}$ curve corresponding to a second-order ferroelastic transition with a 2–4 Landau potential [14]. Thus, it is the *structure* of the T2 rings in unit cells considered in our computer model which yields the local interactions resulting in topological walls.

It would also appear that the cordierite $Q(T)$ plot is closer to a first-order curve than that of the one-atom model. Indeed cordierite has been experimentally observed to show a strong first-order phase transition. However, the accuracy of these results is probably not sufficient to distinguish between first- and second-order transitions so we will merely conclude from this graph that the structure of the T2 rings causes short-ranging interactions to become more important.

Throughout this paper we will plot order parameters as functions of temperature, including those derived from Landau theory, all the way down to $T = 0$ (and for consequently high

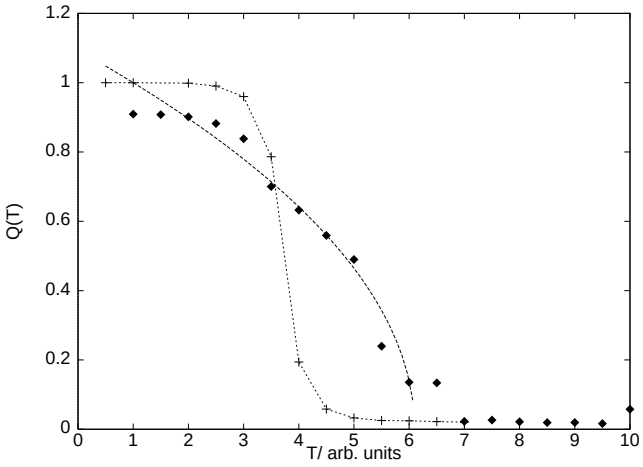

Figure 5. A $Q(T)$ plot for a cordierite simulation (crosses). For comparison, the order parameter of a simple computer model with one atom per unit cell and the same symmetry properties as cordierite is also plotted. The latter curve is similar to a $(T - T_c)^{1/2}$ curve corresponding to a second-order ferroelastic transition with a 2–4 Landau potential. The cordierite plot shows a much sharper cut-off than this, which seems to indicate the importance of short-ranging interactions.

values of the order parameters). Strictly speaking, of course, Landau theory is only valid around $T = T_c$ and for low values of the order parameter. However, Landau theory has been shown experimentally to be valid over a surprisingly large range of order parameter values (up to $Q = 0.9$) for various crystals [14] and here we shall assume, for convenience, that it *is* applicable over all temperatures.

Figure 6 shows the time evolution of the cordierite ring spin configuration from an initial random configuration. We see that domains form and rapidly grow with large domains growing at the expense of smaller ones until the sample consists of only three domains, one of each type. Such a configuration is known as trilling. This aggressive coarsening tendency is very characteristic of cordierite. Whereas other materials, such as YBCO, tend to display 'bar-code' patterns of alternating domains [13,15,16], we see that the simulation never displays this pattern; rather the configuration consists of patchy, irregular domains. This distinction between cordierite and other ferroelastics is present both in our computer simulation compared with computer simulations of these materials and in experimental TEM comparisons of cordierite with these materials. This indicates that the physical process which makes cordierite so unusual has been captured in our simulation.

Looking at the domain walls now, we see that topological walls are dominant on the small length scales associated with short annealing times. For example, in the first snapshot, at $t = 10$ MCSPS, the domains are small and the configuration is entirely made up of topological walls. Later, as coarsening proceeds, the strain walls begin to assert themselves and the large vertical 1–2 wall at $t = 2000$ MCSPS is a strain wall. Some topological walls are still present, however, even at these later times, such as the 1–2 -60° wall at $t = 100$ and the horizontal 2–3 wall at $t = 2000$ MCSPS.

We can see some evidence of wetting along strain-mediated walls. For example, the horizontal 1–2 strain wall to the right of $t = 150$ MCSPS is peppered with type 3 ring spins, giving rise to 1–3 and 3–2 topological domains on a local scale. This wall structure is exactly what we expect for a sandwich wall. The vertical 1–2 wall at $t = 2000$ MCSPS is also wetted by type 3 ring spins.

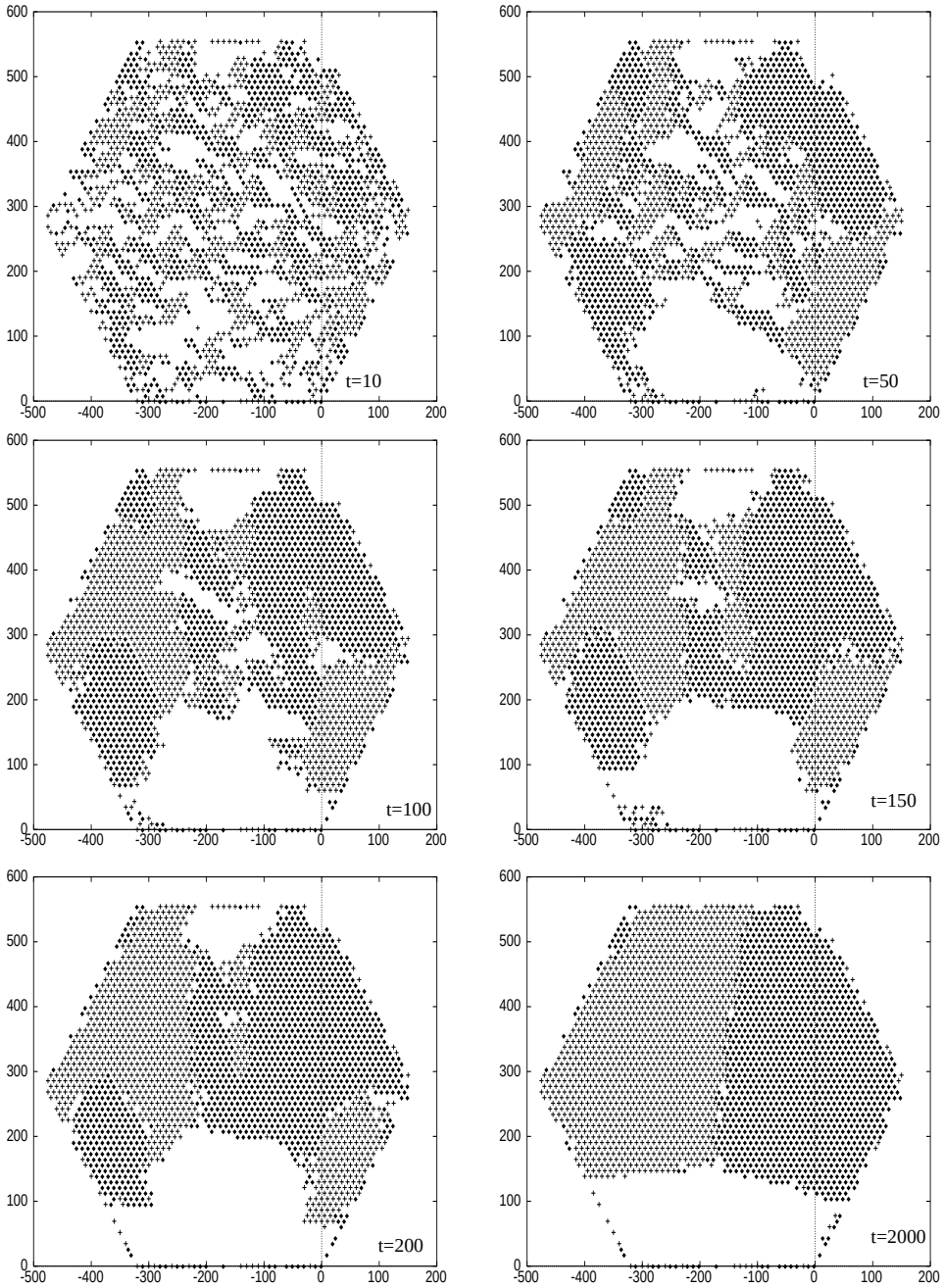

Figure 6. Time (i.e. Monte Carlo) evolution of the system from a random configuration below T_c. Both strain and topological walls are formed.

5. Sandwich walls

In order to understand the behaviour of sandwich walls in more detail, the initial configuration was set to correspond to a sandwich wall precisely as shown in figure 3. The computer

programme was then run at different temperatures. However, rather than simply plotting snapshots such as in figure 6, we now use Ginzburg–Landau theory to gain an understanding of what wall shape is expected.

5.1. Ginzburg–Landau theory

For a symmetry reduction from hexagonal to orthorhombic, the point group of the crystal lattice reduces from $6/mmm$ to mmm and the active representation is E_{2g}. In such a case, the expected form of the Landau potential is given by [17]

$$G = \frac{1}{2}A(q_1^2 + q_2^2) + \frac{1}{3}B(q_1^2 + q_2^2)^{3/2}\cos\left(3\tan^{-1}\frac{q_1}{q_2}\right) + \frac{1}{4}C(q_1^2 + q_2^2)^2. \quad (19)$$

It depends on two components of the order parameter, q_1 and q_2. In the simulation, we only allow orthorhombic cordierite to form (i.e., the ordering-atom configuration is always one of the three possibilities shown in figure 1). This constraint corresponds to setting B very high in the above equation. Thus, the free energy of the system is minimized when the second (angular) term is minimized. This happens when the cosine is equal to -1 which occurs when q_1/q_2 is given by $\pm\sqrt{3}$ or 0. This gives three possible values of the (normalized) vector order parameter $\boldsymbol{q}$:

$$\boldsymbol{q} = (q_1, q_2) = (0, 1), (\pm\sqrt{3}/2, -1/2) \quad (20)$$

which correspond to the three domains that we can observe. Looking at the three strains for such domains using the numbering system of figure 1, with respect to the indicated axes:

$$\begin{aligned}
\mathbf{e}_1 &= e\begin{pmatrix} -1/2 & \sqrt{3}/2 & 0 \\ \sqrt{3}/2 & 1/2 & 0 \\ 0 & 0 & 0 \end{pmatrix} \\
\mathbf{e}_2 &= e\begin{pmatrix} -1/2 & -\sqrt{3}/2 & 0 \\ -\sqrt{3}/2 & 1/2 & 0 \\ 0 & 0 & 0 \end{pmatrix} \\
\mathbf{e}_3 &= e\begin{pmatrix} 1 & 0 & 0 \\ 0 & -1 & 0 \\ 0 & 0 & 0 \end{pmatrix}
\end{aligned} \quad (21)$$

we see that the order parameters are simply the reduced spontaneous strain components, e_{11}/e and e_{12}/e, with

$$\begin{aligned}
e_{11}/e &= q_2 = \sin(\pi/2 - 2\pi/3s) \\
e_{12}/e &= q_1 = \cos(\pi/2 - 2\pi/3s)
\end{aligned} \quad (22)$$

where s is the ring spin value as used in figure 1. Thus, the order parameters for a ring can be calculated from its spin value. As we go through the wall in the x-direction indicated in figure 3, we see that the variation of the order parameters is as shown in figure 7. In a real wall it is expected that gradient energies will smooth off the order parameter profiles. Also shown are the normalized order parameters, Q_1 and Q_2, which are given by

$$Q_1 = (2/\sqrt{3})q_1 \qquad Q_2 = (2/3)(q_2 + 1/2) \quad (23)$$

which give values of $\boldsymbol{Q} = (Q_1, Q_2) = (\pm 1, 0), (0, 1)$ for the three stable bulk configurations expected.

Since the coefficient of B in equation (19) is always set to -1, we can define $G' = G + B$ and write this out as

$$G' = \frac{1}{2}Aq_1^2 + \frac{1}{4}Cq_1^4 + \frac{1}{2}Aq_2^2 + \frac{1}{4}Cq_2^4 + \frac{1}{2}Cq_1^2q_2^2 \quad (24)$$

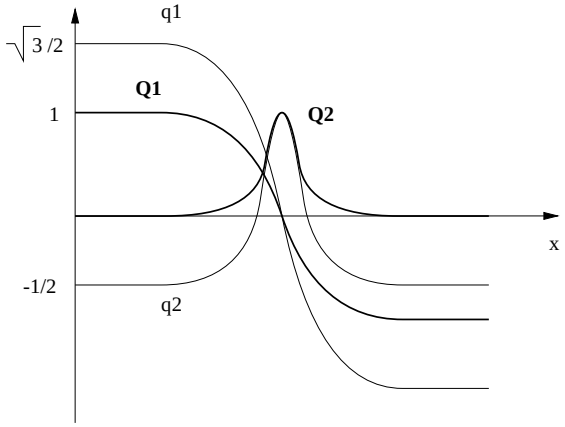

Figure 7. A schematic diagram of the sandwich wall profile in the order parameters.

which is a standard 2–4 potential in q_1 and q_2 with a biquadratic coupling term. There are only two coefficients, A and C, because of symmetry constraints. In addition, we now add Ginzburg terms to provide a gradient energy and integrate the free-energy density to give the total free energy:

$$G' = \int \left[\frac{1}{2}Aq_1^2 + \frac{1}{4}Cq_1^4 + \gamma_1\left(\frac{\partial q_1}{\partial x}\right)^2 + \frac{1}{2}Aq_2^2 + \frac{1}{4}Cq_2^4 + \gamma_2\left(\frac{\partial q_2}{\partial x}\right)^2 + \frac{1}{2}Cq_1^2q_2^2 \right] \mathrm{d}x \qquad (25)$$

where x is a coordinate perpendicular to the wall as indicated in figure 3. In writing the Ginzburg term in this simple way (as a scalar field), we assume that the wall is flat with no twisting.

Firstly, we consider a uniform distribution in which the above gradient terms are zero. It is necessary to find the set of parameters A, C etc which give rise to the bulk values of q_1 and q_2 at $T = 0$. From figure 7 these values are $\sqrt{3}/2$ and $-1/2$ respectively. To explore phase space more thoroughly, we generalize equation (25):

$$G' = \frac{1}{2}A_1q_1^2 + \frac{1}{4}C_1q_1^4 + \frac{1}{2}A_2q_2^2 + \frac{1}{4}C_1q_2^4 + \frac{1}{2}C_2q_1^2q_2^2. \qquad (26)$$

Minimizing this equation gives four solutions for $\boldsymbol{q}$: $(q_1 = 0, q_2 = 0)$, $(q_1 \neq 0, q_2 = 0)$, $(q_1 = 0, q_2 \neq 0)$, $(q_1 \neq 0, q_2 \neq 0)$. Clearly the latter is the one which corresponds to the required ground state. It turns out that the required value of $\boldsymbol{q}$, $=(\sqrt{3}/2, 1/2)$, is obtained when

$$\begin{aligned} A_1 &= -(1/4)(C_2 + 3C_1) \\ A_2 &= -(1/4)(3C_2 + C_1). \end{aligned} \qquad (27)$$

These parameters give rise to $q_1 = \sqrt{3}/2, q_2 = -1/2$ as one minimum. However, the energy of this minimum will only be less than those of the other minima if $C_2 < C_1$, as can be shown by calculating the energies of the four minima of equation (26). If $C_2 > C_1$, then the $q_1 = 0, q_2 \neq 0$ phase has a lower energy. At the critical point where $C_2 = C_1 = C$, we see that $A_1 = A_2 = A = -C_1$ gives the required minimum and this also corresponds to equation (25), with the fixed coefficients which we derived from group theory. However, this critical point is a borderline case and in practice it is necessary to perturb A_1 and A_2 slightly away from A

and C_1 and C_2 away from C:

$$\begin{aligned} A_1 &= A + \delta A_1 \\ A_2 &= A + \delta A_2 \\ C_1 &= C + \delta C_1 \\ C_2 &= C + \delta C_2 \end{aligned} \tag{28}$$

in order to be able to realize the correct ground state. This perturbation implies that the system is somewhat less than hexagonal in its high-symmetry form. In experimental cordierite, this could be due to external stresses, defects, finite-size effects and edge effects in the sample. In the computer simulation, edge and finite-size effects will cause the symmetry reduction. The free-energy expression for a non-uniform distribution is therefore given by

$$G' = \int \left[\frac{1}{2}A_1 q_1^2 + \frac{1}{4}C_1 q_1^4 + \gamma_1 \left(\frac{\partial q_1}{\partial x} \right)^2 + \frac{1}{2}A_2 q_2^2 + \frac{1}{4}C_1 q_2^4 + \gamma_2 \left(\frac{\partial q_2}{\partial x} \right)^2 + \frac{1}{2}C_2 q_1^2 q_2^2 \right] \mathrm{d}x. \tag{29}$$

We may now use the calculus of variations to write PDEs for the order parameters as the system approaches its minimum free energy:

$$\begin{aligned} \frac{\partial q_1}{\partial t} &= -\frac{\delta G'}{\delta q_1} = \gamma_1 \frac{\partial^2 q_1}{\partial x^2} - A_1 q_1 - C_1 q_1^3 - C_2 q_1 q_2^2 \\ \frac{\partial q_2}{\partial t} &= -\frac{\delta G'}{\delta q_2} = \gamma_2 \frac{\partial^2 q_2}{\partial x^2} - A_2 q_2 - C_1 q_2^3 - C_2 q_1^2 q_2 \end{aligned} \tag{30}$$

with the boundary conditions

$$\begin{aligned} \left[\frac{\partial q_1}{\partial x} \right]_{x=\pm\infty} &= 0 \\ \left[\frac{\partial q_2}{\partial x} \right]_{x=\pm\infty} &= 0. \end{aligned} \tag{31}$$

We now proceed to solve these equations numerically using an Euler method. The sample is divided into grid points and the derivatives in equation (30) are written using finite differences. C_1 is taken to be 1 and C_2 is 0.9 (so C_2 is less than but close to C_1 as required). From equation (27), this gives $A_1^0 = -0.975$ and $A_2^0 = -0.925$ at $T = 0$.

Both A_1 and A_2 vary with temperature as

$$\begin{aligned} A_1 &= A_1'(T - T_c) = A_1^0(1 - T/T_c) \\ A_2 &= A_2'(T - T_c) = A_2^0(1 - T/T_c) \end{aligned} \tag{32}$$

so the ratio $A_1/A_2 = A_1^0/A_2^0$ is constantly equal to 39/37. In the computer simulation, we use the values of A_1 and A_2 given in table 2.

Table 2. Values of A_1 and A_2 used in the simulation.

A_1	−0.975	−0.800	−0.600	−0.400	−0.200	−0.100
A_2	−0.925	−0.759	−0.569	−0.379	−0.190	−0.095

Finally, we must choose values of the Ginzburg coefficients, γ_1 and γ_2. The parameter which varies as a result of the formation of a sandwich wall but which is fixed in a strain wall is q_2. Therefore in order to encourage the formation of a sandwich wall we must set $\gamma_2 < \gamma_1$. Physically this means that topological walls form more readily than strain walls which is indeed

observed to be the case in the computer simulations of the atomistic model. We therefore set $\gamma_1 = 1$ and $\gamma_2 = 0.2$. At higher values of γ_2 the sandwich wall does not form.

The initial configuration used in the simulation was a hyperbolic tangent function for q_1 and a Gaussian peak for q_2 inside the wall. Figure 8 shows the final, converged distributions of the order parameters for the different A-coefficients listed above. In each case, the program was run until the free energy had reached its minimum to five decimal places and the order parameter plots had converged to those shown in the figure.

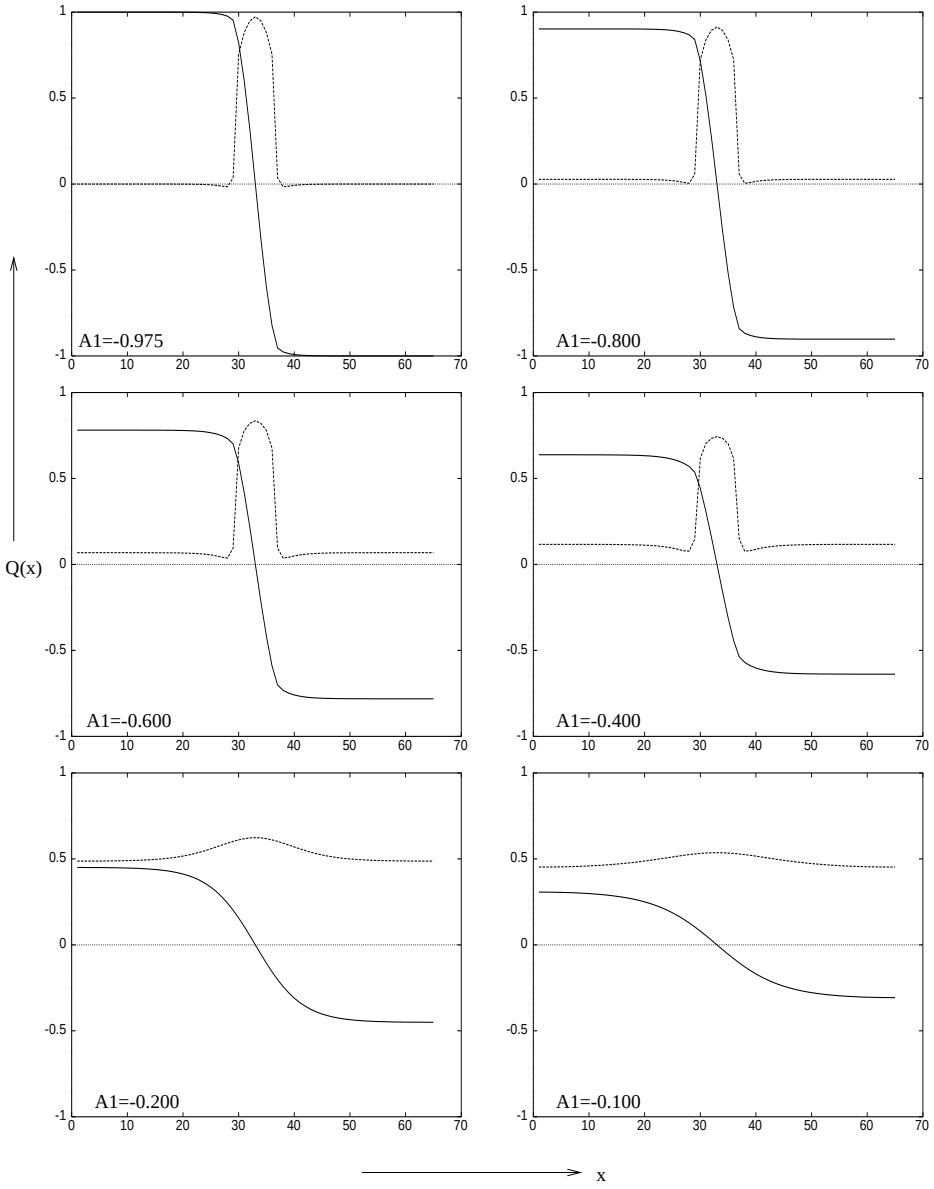

Figure 8. Final (converged) order parameter plots at different temperatures. The expected sandwich wall is stable until $A_1 = -0.4$ but then changes into another form at higher temperatures (see the text).

We see that the choice of parameters does indeed give $\boldsymbol{Q} = (\pm 1, 0)$ in the bulk at $T = 0$, $A_1 = -0.975$ and there is a peak in Q_2 at the sandwich wall. If Q_2 were set at zero, then there would be no coupling and the Q_1-curve would be a hyperbolic tangent function with width $\propto 1/(T_c - T)$. In the $T = 0$ solution, however, Q_1 is considerably distorted away from such a curve by the high value of Q_2 in the wall. In fact Q_2 almost reaches its saturated value of 1. Rather than being Gaussian shaped, the Q_2-peak has a rounded tip and there is a dip in Q_2 at its base.

As temperature is increased, both order parameter maximum values decrease but their widths remain approximately constant. The value of Q_2 in the bulk (away from the wall) increases somewhat. Bearing in mind that $q_2 = (1/2)(3Q_2 - 1)$, it can be seen that the strain component $e_{11} \propto q_2$ continues to change sign inside the wall as expected. However, between $A_1 = -0.4$ and -0.2, a phase transition occurs above which the sandwich wall takes on a new profile. In this latter configuration, Q_1 is much closer to the expected hyperbolic tangent profile and its width does change with temperature. Q_2 is much flatter and less sharp and resembles a Gaussian distribution. Figure 9 shows the time evolution of the system as it moves away from its initial configuration and adopts that shown in figure 8.

Returning to figure 8, we observe that, at $A_1 = -0, 2, -0.1$, Q_2 is above $1/3$ both inside and outside the wall, indicating that q_2 and hence also e_{11} do not change sign as we move across the wall. Certainly a configuration whereby three domains are placed together without interacting with each other should have e_{11} changing sign like this: $-1/2$, 1, $-1/2$. Although such a strain configuration is observed at low temperatures, it appears that the more rapid thermal fluctuation at high temperatures causes the system to escape from such a configuration and adopt a new state with e_{11} positive in the bulk and becoming *more* positive in the wall. So the strain component is not even attempting to change its sign but doing the opposite. This configuration still has $e_{12} = 0$ inside the wall, however: it is just that the direction of the stretching and contraction in the wall have now reversed.

Bulk values of Q_1 simply decrease with temperature to zero at $T = T_c$, while the bulk value of Q_2 first increases towards its infinite-temperature limit of $1/3$, then jumps above $1/3$ as the transition point inherent in figure 8 is passed, then decreases to $1/3$ with further increases of temperature. Trajectories of Q_1 versus Q_2 at these temperatures are shown in figure 10.

These sandwich walls are examples of *chiral walls*, so called because the order parameter $\boldsymbol{Q}$ rotates as we move through the wall. The direction of rotation indicates the chirality of the wall. In equation (19), the free energy depends only on the *squares* of the order parameters q_1 and q_2, so the sign of the order parameters is irrelevant. Houchmandzadeh *et al* [7] described how this would lead to degeneracy between positive and negative chiral walls. However, in our system the order parameters are linked to the strain components via equation (22), so the signs of q_1 and q_2 *are* significant. For example, if (at $T = 0$) we again allowed q_1 to go from $\sqrt{3}/2$ to $-\sqrt{3}/2$ along x (as in figure 7) but had q_2 going as $+1/2$, -1, $+1/2$, the signs of e_{11} would change producing strains:

$$e\begin{pmatrix} 1/2 & \sqrt{3}/2 & 0 \\ \sqrt{3}/2 & -1/2 & 0 \\ 0 & 0 & 0 \end{pmatrix} \qquad e\begin{pmatrix} 1/2 & -\sqrt{3}/2 & 0 \\ -\sqrt{3}/2 & -1/2 & 0 \\ 0 & 0 & 0 \end{pmatrix} \tag{33}$$

in the bulk (outside the sandwich wall). However, only the strains in equation (21) are energy allowed in the bulk, and e is fixed by the strengths of the interactions between the atoms. Therefore the two types of chirality are not degenerate in our system and the chirality of figure 10 gives the energy minimum. The fact that the GL equations shows the chiralities to be degenerate is due to the approximations involved in formulating these equations.

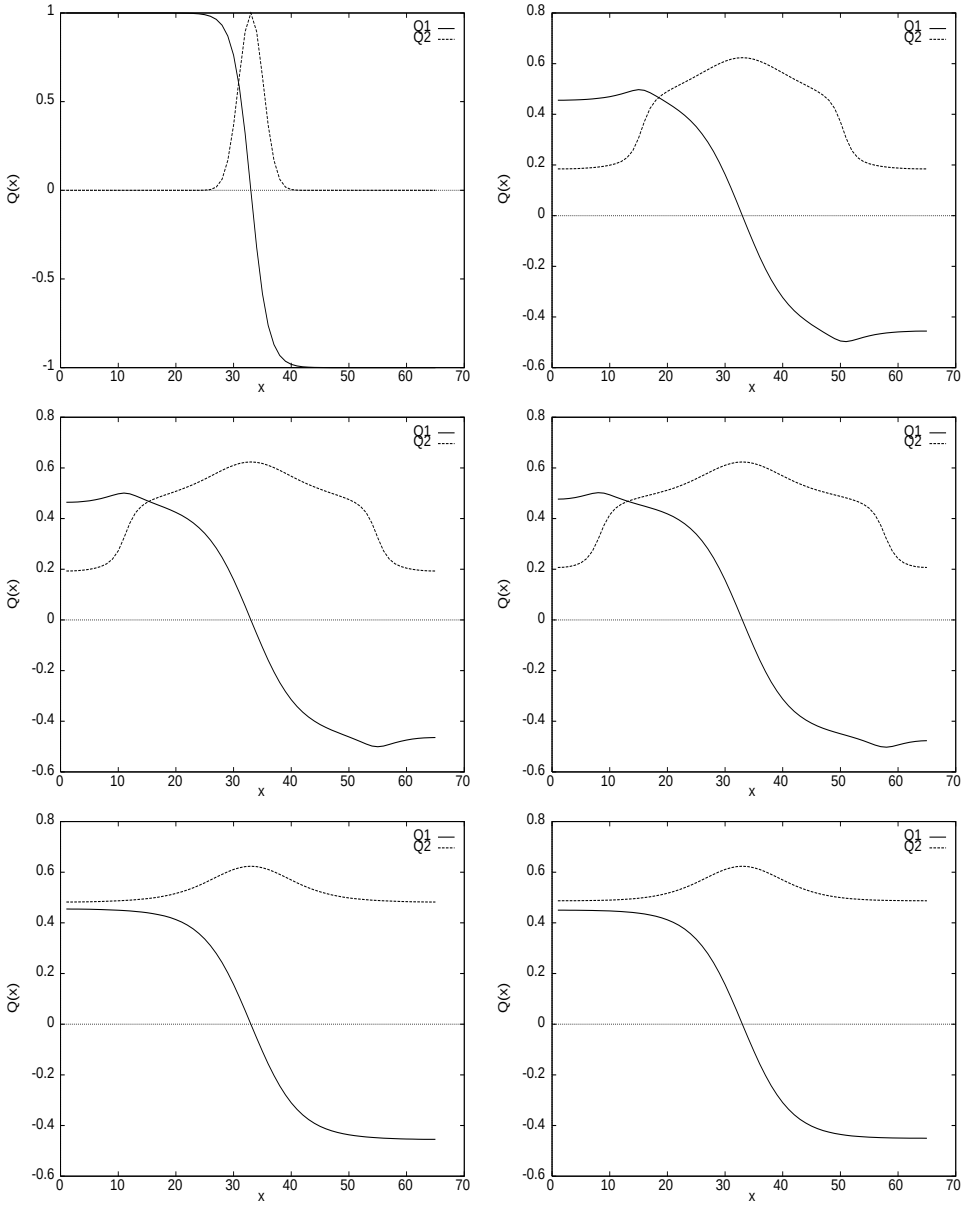

Figure 9. Time evolution of order parameters at $A_1 = -0.2$. At this temperature the system moves away from the expected strain configuration and adopts a different strain inside the wall (see the text). The sequence is from left to right and top to bottom.

5.2. Atomistic simulation

We now calculate wall trajectories for the full atomistic simulation. The system is set up initially with the configuration shown in figure 3 (i.e. with a single sandwich wall) and run at several temperatures. The order parameters Q_1 and Q_2 are calculated for each T2 ring from equations (22) and an average is taken over horizontal rows to yield $Q_1(x)$ and $Q_2(x)$. Notice

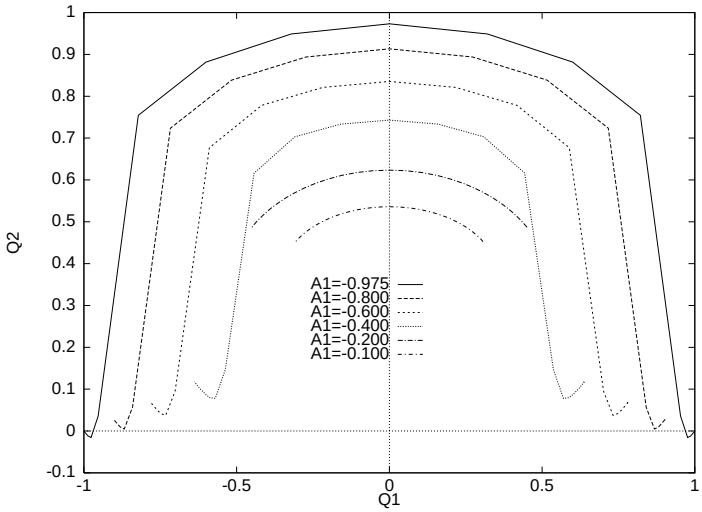

Figure 10. Q_1–Q_2 trajectories for a variety of temperatures (i.e. values of A_1 and A_2). The parameter $\boldsymbol{Q}$ goes from right to left in each case.

that although the Q-values for each ring are fixed at one of three values, the functions $Q_1(x)$ and $Q_2(x)$ can vary smoothly due to the averaging process. Walls are locally sharp (we are either in one domain or another with no in-between state) but are globally smooth when many ring spins are averaged in this way.

In order to improve the statistics, the order parameters were also averaged over Monte Carlo steps as the simulation was run. Each simulation was run for 1000 MCSPS. The results are shown in figure 11 which also shows representative snapshots at the various temperatures after thermal equilibrium has been reached.

At low temperatures, $T < 2$ (with $T_c = 4$ from figure 5), the system just stays at the initial configuration with all Monte Carlo rotations of Al pairs being rejected. This clearly shows that the topological walls are entirely stable in this system as expected from their spontaneous appearance in figure 6. However, by $T = 2$ there is some observed fluctuation and, as expected, the order parameters round off to form an approximate hyperbolic tangent function of Q_1. Q_2 remains at zero outside the wall as required, but peaks inside the wall. We notice however that the peak is rather small compared to that of the Landau theory results in figure 8. Looking at a representative snapshot of the ring spin configuration, we see that the amount of type 3 wetting along the wall is indeed rather small and much off it is near the edges of the sample. As the temperature is increased towards T_c, the bulk value of Q_1 decreases towards zero and the bulk value of Q_2 increases towards $1/3$ as expected. Perhaps because of the small Q_2-peak here, the order parameter curves seem to more closely resemble hyperbolic tangent and Gaussian curves than in the Landau theory simulation and their widths clearly increase with temperature. This is reasonable because the hyperbolic tangent curve is expected in the limit as $Q_2 \to 0$. By $T = 4$, Q_1 and Q_2 are close to their infinite-temperature values but the peak in Q_2 is still present. The order parameters retain rather high values at the edges of the sample due to edge effects.

The small size of the Q_2-peak may be due to cordierite's aggressive coarsening tendency which results in small domains being eaten up by nearby larger ones. Thus, there is a competition between two processes: type 3 ring spins forming in the wall in order to give rise to topological walls; and these spins turning back into type 1 and type 2 spins in order to

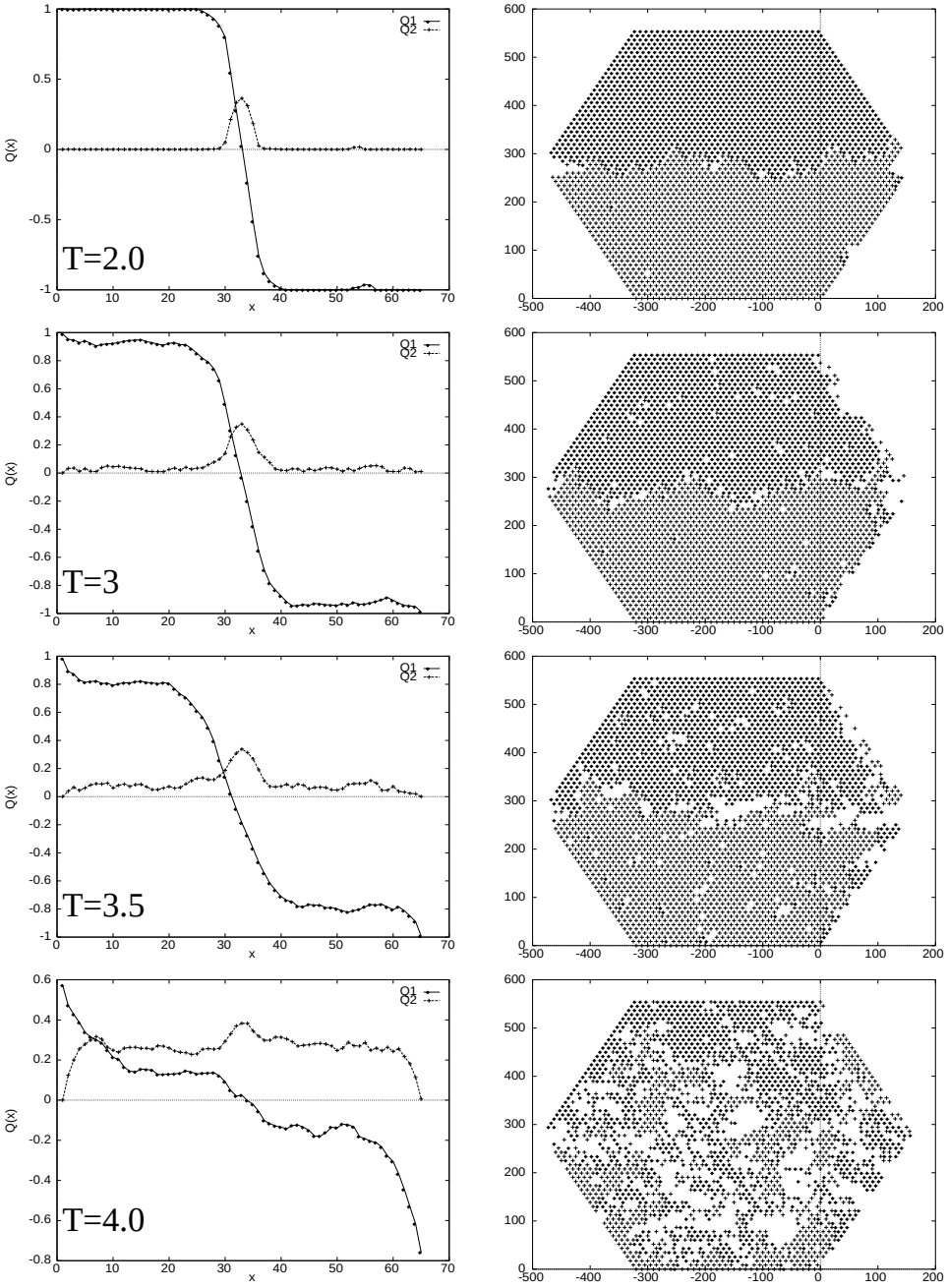

Figure 11. Averaged order parameter distributions for the full, atomistic model at various temperatures. Representative ring spin snapshots are also shown at each temperature.

join with the two large domains. Indeed there appear to be two regimes: at low temperatures, the type 3 sandwich filling is a stable domain, whereas at $T \geqslant 2$, as shown in figure 11, the type 3 ring spins form a thin wetting layer between two domains (type 1 and 2). This latter effect is reminiscent of surface segregation whereby a third species type can nucleate

preferentially at the interface between the other two species [18–25].

The phase transition observed in the Landau simulation (between $A_1 = -0.4$ and -0.2) is not observed here, since the ring spin values rather than the strains are averaged to give these plots. A strain profile was plotted corresponding to the spin configuration at $T = 2$ in figure 11 and gave the expected strains (with e_{11}/e going as $-1/2, 1, -1/2$). At higher temperatures, the rapid fluctuations make it computationally impossible to calculate strain profiles sufficiently accurately, so this phase transition cannot be directly confirmed here.

6. Conclusions

Cordierite has unusually low anisotropy energies and a low spontaneous strain. Therefore other interactions between ordering atoms become important, including local interactions between cordierite's characteristic sixfold rings. This latter process gives rise the formation of topological walls as well as the expected strain walls and there is a competition between these two wall types. A compromise 'sandwich wall' which consists of both strain and topological walls is therefore a low-energy solution. Such a wall is shown to be stable by using both symmetry-adapted Ginzburg–Landau theory and our atomistic model. Plots of the order parameter at low temperatures show the expected variation in strains between the three different domains which comprise the sandwich wall. However, at higher temperatures, the GL theory yields a wall with the 'filling' in the sandwich being stretched in the other direction to that of the stretching which occurs at low temperatures (the shear strain remains at zero). The atomistic simulation is unable to confirm this last prediction because of poor statistics. However, the mapping between the two simulations at low temperatures is sufficiently convincing to make this latter prediction seem plausible.

The exact distribution of the sandwich filling is interesting and varies with temperature from a well defined slab at low temperature to a thin wetting layer at higher temperatures more reminiscent of surface segregation phenomena.

The sandwich wall is a result of the competition between two wall types and also cordierite's unusual triple-domain structure. Most other ferroelastics have only two domains and so cannot support a sandwich wall.

References

[1] Sapriel J 1975 *Phys. Rev.* B **12** 5128
[2] Fousek J and Janovec V 1969 *J. Appl. Phys.* **40** 135
[3] Janovec V 1976 *Ferroelectrics* **12** 43
[4] Venkatesh V 1954 *Am. Mineral.* **39** 636
[5] Muller W F and Schreyer W 1991 *Eur. J. Mineral.* **3** 915
[6] Blackburn J F and Salje E K H 1999 *Phys. Chem. Minerals* **26** 275
[7] Houchmandzadeh B, Lajzerowicz J and Salje E 1991 *J. Phys.: Condens. Matter* **3** 5163
[8] Putnis A 1992 *Introduction to Mineral Sciences* (Cambridge: Cambridge University Press)
[9] Eichhorn K and Binder K 1996 *J. Phys.: Condens. Matter* **8** 5209
[10] Binder K 1981 *J. Stat. Phys.* **24** 69
[11] Thayaparam S, Heine V, Dove M T and Hammonds K D 1996 *Phys. Chem. Minerals* **23** 127
[12] Tsatskis I and Salje E 1996 *Am. Mineral.* **81** 800
[13] Bratkovsky A M, Marais S C, Heine V and Salje E K H 1994 *J. Phys.: Condens. Matter* **6** 3679
[14] Salje E 1993 *Phase Transitions in Ferroelastic and Coelastic Crystals* (Cambridge: Cambridge University Press)
[15] Putnis A and Salje E 1994 *Phase Transitions* **48** 85
[16] Bratkovsky A M, Salje E K H, Marais S C and Heine V 1994 *Phase Transitions* **48** 1
[17] Salje E 1987 *Phys. Chem. Minerals* **14** 455
[18] Hammer M, Monty C, Endriss A and Hoffmann M J 1998 *J. Am. Ceram. Soc.* **81** 721
[19] Pertsev N A and Emelyanov A Y 1997 *Phys. Solid State* **39** 109

[20] Aaberg R J, Tunold R, Mogensen M, Berg R W and Odegard R 1998 *J. Electrochem. Soc.* **145** 2244
[21] Esch F, Gunther S, Schutz E, Schaak A, Kevrekidis I G, Marsi M, Kiskinova M and Imbihl R 1998 *Catal. Lett.* **52** 85
[22] Carlsson A, Clasesson D, Katrich G, Lindgren S A and Wallden L 1998 *Phys. Rev.* B **57** 13 192
[23] Lojkowski W, Rabkin E, Straumal B, Shvindlerman L S and Gust W 1998 *Defect Diffusion Forum* **156** 163
[24] Glickman E E 1998 *Defect Diffusion Forum* **156** 147
[25] Hong S H, Lee N, Carim A H and Messing G L 1998 *J. Mater. Res.* **13** 974